

# Photovoltaic performance of c-Si wafer reclaimed from end-of-life solar cell using various mixing ratios of HF and HNO<sub>3</sub>



Jun-Kyu Lee<sup>a,c</sup>, Jin-Seok Lee<sup>a,\*</sup>, Young-Soo Ahn<sup>a</sup>, Gi-Hwan Kang<sup>b</sup>, Hee-Eun Song<sup>b</sup>, Jeong-In Lee<sup>b</sup>, Min-Gu Kang<sup>b</sup>, Churl-Hee Cho<sup>c,\*\*</sup>

<sup>a</sup> Advanced Materials and Devices Laboratory, Korea Institute of Energy Research, Daejeon 305-343, Republic of Korea

<sup>b</sup> Photovoltaic Laboratory, Korea Institute of Energy Research, Daejeon 305-343, Republic of Korea

<sup>c</sup> Graduate School of Energy Science and Technology, Chungnam National University, Daejeon 305-764, Republic of Korea

## ARTICLE INFO

### Keywords:

End-of-life solar cell  
Recovery  
Silicon wafer  
Solar cell  
Efficiency

## ABSTRACT

This study presents the re-fabrication of a crystalline silicon (c-Si) solar cell using a Si wafer reclaimed from the solar cell of an end-of-life (EoL) module, and an evaluation of its performance. A 6-in. commercial solar cell was used in the etching process by wet chemical process in order to investigate the optimal mixing ratio of a mixture of HNO<sub>3</sub> and HF. The silicon nitride (SiN<sub>x</sub>) and aluminum (Al) back contact on both sides of the solar cell were not completely removed at a high ratio of aqueous HNO<sub>3</sub>, and the precipitation of Ag particles on the surface of Si wafer were deposited at a high ratio of aqueous HF in a mixed acid solution. The optimum etching condition for the recovery of the c-Si wafer was applied to the EoL module, which consisted of 4" solar cells. The photovoltaic (PV) performance of the re-fabricated 4" solar cell was measured by conventional solar cell processing, which shows the best results reported so far. The higher boron (B) concentration and reflectance of the re-fabricated solar cell reduced cell efficiency by 0.6% compared with the commercial 6" solar cell. However, it has sufficient potential for use in the PV industry.

## 1. Introduction

Photovoltaics (PVs) involve the use of sunlight as a clean and sustainable energy resource, which is the most representative of renewable energy sources [1]. Global PV capacity has been increasing steadily over the last fifteen years, reaching 177 GW by 2014 (with the addition of 38.7 GW in 2014 alone), *i.e.* at least ten times more than the figure recorded in 2008 [2]. The continuing development of the PV industry has led to a high portion for crystalline silicon (c-Si) solar cells, and c-Si modules have been widely installed worldwide. The market share of global c-Si PV modules is assumed to have remained unchanged at around 85–90% [3]. Despite a dramatic rise in the installation of PV modules, they cannot be used any longer than about 25–30 years because they incur such damages as cracks in the cells, delamination, EVA discoloration, burn marks, potential induced degradation, and so on [4], which results in their being discarded despite the environmental issues. Therefore, the recycling of PV modules has received considerable attention as a proper way of treating end-of-life (EoL) PV modules [5–7]. There are numerous reports on the recycling of EoL PV modules [8–12], and even the European Union announced

the Guideline 2012/19/EU in order to fix the regulations on the disposal of EoL PV modules [13]. In accordance with this guideline, EoL PV modules are officially regarded as waste electrical and electronic equipment (WEEE), which means used PV modules must be collected and recycled [14]. c-Si solar cell modules are composed of low iron glass, an aluminum (Al) frame, a solar cell, an encapsulant (generally EVA), a back-sheet, and a junction box, in order of mass. Of these components, the Al frame and junction box can be mechanically dismantled more easily than the other components. However, recovering of unbroken solar cell from PV module is very difficult. Therefore, advanced thermal process is required in order to recover the unbroken solar cells [15]. The recovery of c-Si wafers from unbroken solar cells is considered worthwhile because the c-Si wafering process accounts for more than 65% of the production cost of solar cells [16]. As such, it is possible to manufacture PV modules at a lower cost by using the c-Si wafers reclaimed from EoL solar cells. However, conventional wet chemical processes involving more than two steps are required in order to remove certain solar cell components – such as the anti-reflection (AR) layer, emitter layer, and the front and back contacts – and to recover c-Si wafers from EoL solar cells, as well as many chemical

\* Corresponding author.

\*\* Corresponding author.

E-mail addresses: [jslee@kier.re.kr](mailto:jslee@kier.re.kr) (J.-S. Lee), [choch@cnu.ac.kr](mailto:choch@cnu.ac.kr) (C.-H. Cho).

solvents and rising processes [17–19]. In this research, a mixture of acid solvents was used to recover the mono c-Si wafer by varying the mixing ratios of the solvents. The mixing ratio of acids is the most important parameter for efficiently removing functional layers on both sides of a c-Si solar cell, because each acid has a different chemical reaction with each of the different materials in the cell. Finally, the optimum process condition for the recovery of c-Si wafers was applied to the EoL module consisting of 4" solar cells. In addition, the PV performance of the re-fabricated 4" solar cell was measured by conventional solar cell processing, which shows the best results reported so far.

## 2. Experimental procedure

### 2.1. Acid leaching

6" mono c-Si commercial solar cells with three bus bars were used in an optimizing study of the acid leaching condition. The chemical etching process for recovering c-Si wafers from solar cells consisted of only one step, *i.e.* the simultaneous removal of the front and back electrodes, AR coating, and emitter layer. The solar cells were immersed in a mixture of 20 wt% HNO<sub>3</sub> and 20 wt% HF for 6 min at room temperature. As shown in Table 1, the mixing ratios of HNO<sub>3</sub> and HF were varied at 92:8, 83:17, 67:33 and 50:50, and named as samples A, B, C and D. The temperature increased up to around 100 °C during the chemical reaction because the chemical process led to a strong exothermic reaction. Also, the stirring effect was generated by the formation of a lot of bubbles in the bath during the chemical reaction between solar cell and mixed acid solution. A rinse in deionized water was required after etching process.

In order to recover unbroken c-Si solar cell from the 4" EoL module, we employed a method reported in a previous work [15]. Then, the optimal experimental condition was applied to a 4" solar cell recovered from an EoL solar cell in order to reclaim the c-Si wafer. A scanning electron microscope (SEM; Hitachi S-4700) and an energy dispersive X-ray spectroscopy (EDS; Horiba EMAX 7200-H) were employed to investigate the surfaces, thickness, and residual elements of the reclaimed c-Si wafer. The concentrations of boron (B) and phosphorus (P) of the reclaimed wafer were measured using a glow discharge mass spectrometer (GDMS; Thermo VG 9000).

### 2.2. Re-fabrication of solar cells

The B-doped (100) p-type c-Si wafer reclaimed from an EoL solar cell had an area of 100×100 mm<sup>2</sup> (4 in.), a thickness of 240 μm, and resistivity of 0.5–3 Ω cm. The wafer was textured in a mixed solution of KOH:isopropanol at 88 °C and etched by ~4 μm on each side. Then, the emitter was formed *via* a gaseous diffusion from a phosphorous oxychloride (POCl<sub>3</sub>) source in a tube furnace. After thermal diffusion and the subsequent phosphosilicate glass (PSG) removal in an HF solution, sheet resistance of ~50 Ω/sq was measured using a 4-point probe. An AR coating (SiN<sub>x</sub>:H) was deposited *via* plasma-enhanced chemical vapor deposition (PECVD) using silane, ammonia, and argon gases. The thickness of the AR coating was 760–770 Å, and the refractive index was 2.1 at 630 nm. This coating also functioned as the surface passivation layer. The front and back electrodes were formed *via* a screen-printing method using silver (Ag) and Al pastes, respectively. After printing with the metal paste and drying, the wafer

**Table 1**  
Experimental etching conditions in a mixture of HNO<sub>3</sub> and HF solution.

Sample	A	B	C	D
Mixing ratio (HNO <sub>3</sub> : HF)	92: 8	83: 17	67: 33	50: 50
Etching time	6 min			

was co-fired in an IR lamp-heated belt furnace in order to form the ohmic contact between the metal and the semiconductor. Because the wafer was doped on both sides, edge isolation was applied using a 532 nm Q-Switched Nd:YVO<sub>4</sub> laser. The current-voltage characteristic of the re-fabricated solar cell was obtained using a solar simulator (McScience K210 LAB160). In this paper, COM and REC indicate a 6" commercial mono c-Si wafer-based solar cell and a 4" reclaimed mono c-Si wafer-based solar cell from an EoL solar cell, respectively. For comparison, the two wafers were treated by same cell processing.

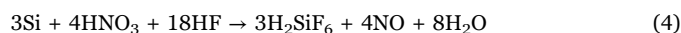
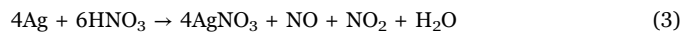
## 3. Results and discussion

### 3.1. Behavior of acid leaching

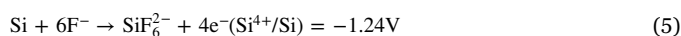
The chemical etching behaviors of the front and back surfaces of the Si wafers reclaimed from 6" solar cells, according to the various mixing ratios of HNO<sub>3</sub> and HF, are shown in Fig. 1. It shows the different surface characteristics in accordance with the experimental conditions. In Fig. 1(a) the Si surface is exposed with a dark grey color, which looks darker than a general Si wafer; in addition, the Al electrode seems to remain on the etched wafer. Meanwhile, in Fig. 1(c), (d), (g) and (h) the etched wafer seems to be stained with something. In addition, Fig. 1(d) and (h) show that the surface of the wafer was changed to a brown color. On the other hand, Fig. 1(b) and (f) show that both the front and back surfaces of the Si wafer were exposed. In order to investigate the different surface characteristics of the samples, as shown in Fig. 1, the front and back surfaces of the etched Si wafers were analyzed by SEM, as shown in Fig. 2. Fig. 2(a) and (e) show that there were detached layer and surfaces round metallic particles, respectively. Fig. 2(c), (d), (g) and (f) show very small particles on the surface of the etched wafers. On the other hand, Fig. 2(b) and (f) show the etched wafers with a relatively smooth and clean surface. In order to more clearly confirm the trace materials on the surface of the etched wafers, EDS analysis was carried out, the results of which are shown in Table 2. In Table 2(a) and (e), the nitrogen (N) and Al (except for Si and oxygen (O)) are considered to be traces of SiN<sub>x</sub> and the Al back electrode. Generally, SiN<sub>x</sub> and Al were etched by aqueous HF acid according to reactions (1) and (2) [20].



This means that the amount of aqueous HF acid in the mixed solution was insufficient to remove the SiN<sub>x</sub> and Al electrode. For this reason, both the N and Al remained on the etched wafer, as shown in Table 2(a) and (e). The Ag as front electrode was dissolved by aqueous HNO<sub>3</sub> acid according to reaction (3) [21]. The Si wafer was etched by aqueous HNO<sub>3</sub> and HF acids according to reaction (4) [22]:



On the other hand, the Ag element on the etched Si wafers was analyzed, as shown in Table 2(c), (d), (g) and (h), except for Si and O. It confirmed the SEM images, in which Ag particles were observed on the entire surface of the etched wafers, as shown in Fig. 2(c), (d), (g) and (h). This is because the Ag particles were chemically formed on the surface of the Si wafer in an HF/AgNO<sub>3</sub> solution [23]. In a solid state, the Ag was dissolved according to reaction (3), while the revealed Si wafer by aqueous HF acid was etched in a mixed solution according to reaction (4). Accordingly, the deposition of Ag on the Si wafer can be occurred by the following reactions [24].



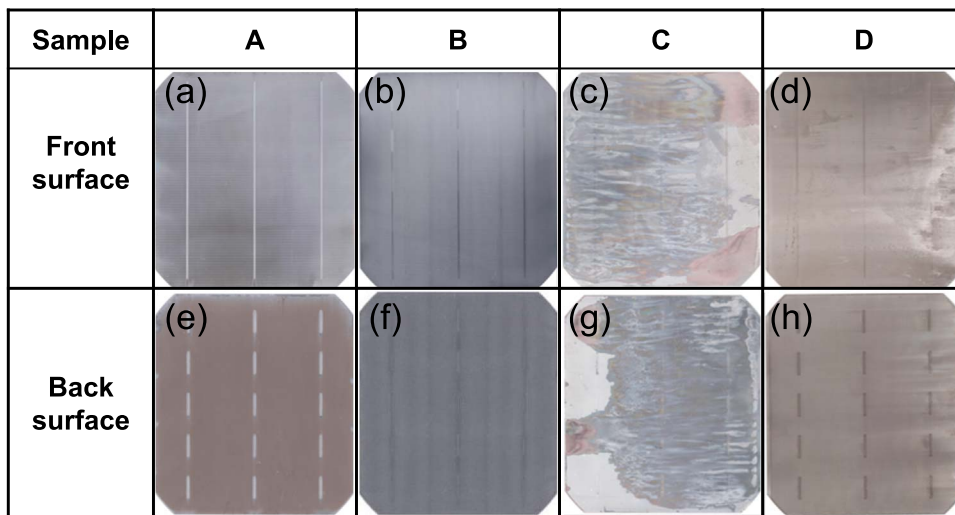


Fig. 1. Pictures of the etched wafers with various mixing ratios of HNO<sub>3</sub> and HF: (a) and (e) 92:8; (b) and (f) 83:17; (c) and (g) 67:33; (d) and (f) 50:50.

Overall reaction is:



From the above reaction, Ag deposition could occur on the entire surface of the Si. It is well known that the electronegativity of Ag is greater than that of Si, it could be attraction electron from Si to become negatively charged [25]. Consequently, Ag particles are deposited on the c-Si wafer during the chemical etching process. On the other hand, Ag was not detected in the result of EDS analysis, as shown in Table 2(b) and (f). This is due to the suitable ratio of mixed acids. In other words, the Ag particles deposited on the surface of the Si wafer by reaction (7) were dissolved by a sufficient amount of aqueous HNO<sub>3</sub> in the mixed solution. As the ratio of aqueous HNO<sub>3</sub> in the mixed solution decreased, the amount of detected Ag showed a significant increase. However, an excessive amount of aqueous HNO<sub>3</sub> in the mixed solution was not etched the SiN<sub>x</sub> and Al electrode. The amount of Ag detected on the front side was greater than the amount on the back side of the Si wafer, as shown in Table 2, because most of the Ag was present on the front surface of the solar cell as front electrode.

### 3.2. Re-fabrication of new solar cell

Fig. 3 shows pictures of the recovered solar cell, the Si wafer

Table 2

Results of the EDS analysis of the etched front and back surfaces of samples A, B, C and D.

Sample	A	B	C	D
<b>Front surface</b>	(a)	(b)	(c)	(d)
N	6.65	–	–	–
O	2.84	3.25	2.57	8.24
Si	90.51	96.75	83.85	50.94
Ag	–	–	13.58	40.82
<b>Back surface</b>	(e)	(f)	(g)	(h)
Al	18.94	–	–	–
O	26.18	2.55	2.60	4.26
Si	54.88	97.45	92.52	72.55
Ag	–	–	4.88	23.19

reclaimed by the chemical etching process, and the re-fabricated new solar cell. The suggested optimization etching process enables the etching of the 4" EoL solar cell. The thickness of wafer has an effect on the PV performance. However, it is well known that the efficiency of Si solar cell is not dependent on the thickness if the wafer thickness is more than 200 μm [26]. The thickness of the reclaimed Si wafer was around 240 μm. For this reason, it was not necessary to consider the effect of the wafer thickness on the PV efficiency. The c-Si wafer

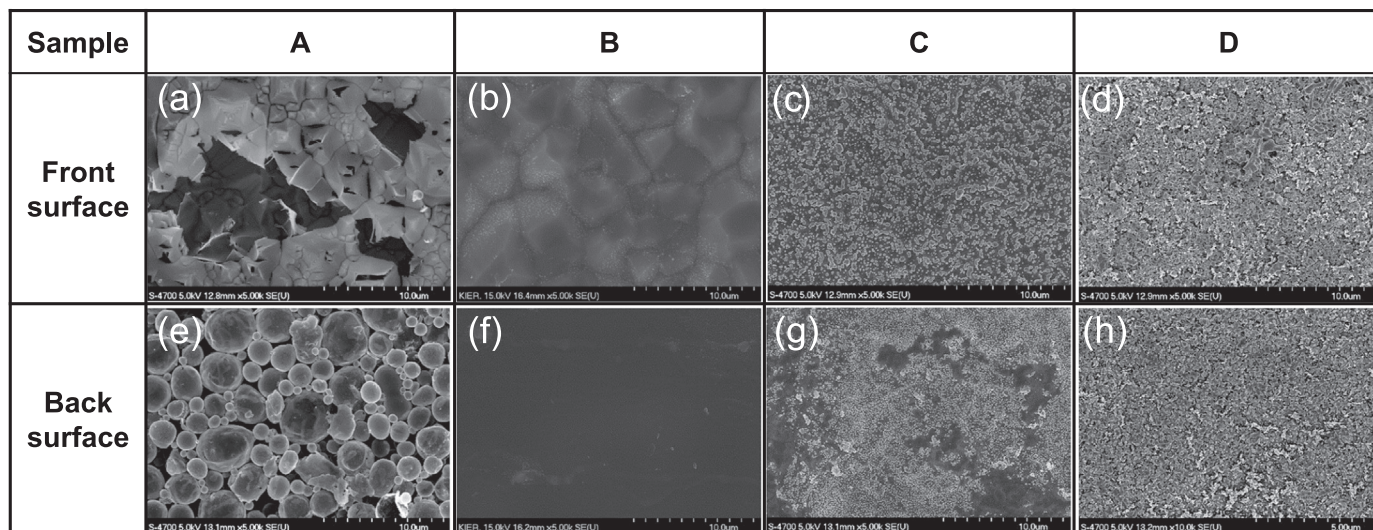


Fig. 2. SEM images of the etched wafers with various mixing ratios of HNO<sub>3</sub> and HF: (a) and (e) 92:8; (b) and (f) 83:17; (c) and (g) 67:33; (d) and (f) 50:50.

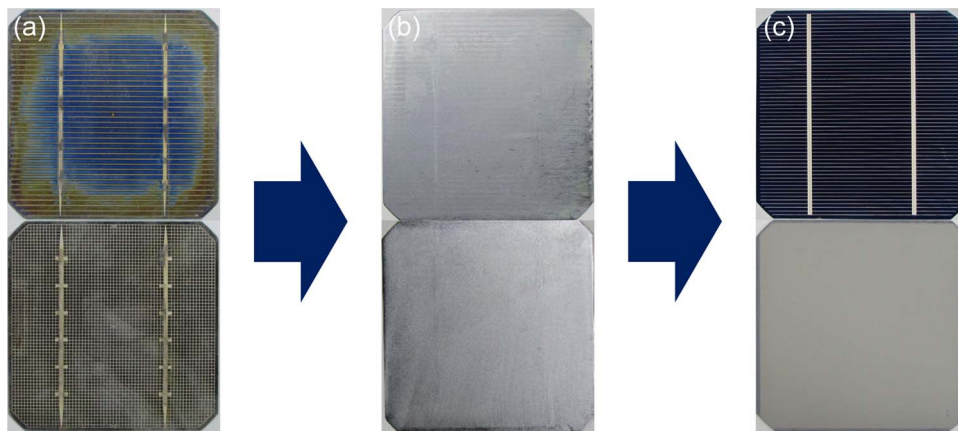


Fig. 3. Pictures of the overall process of chemical etching-based 4" c-Si solar cell from EoL solar cell: (a) EoL solar cell; (b) Reclaimed c-Si wafer; (c) Re-solar cell.

obtained from the chemical etching process was applied to the commercial solar cell fabrication process; and the new solar cell was fabricated based on conventional solar cell processing. The PV performance of the re-fabricated 4" solar cell was significantly improved, rising from an original rate of efficiency of 14.8% to a higher rate of 17.6%.

### 3.3. Light I-V curve

There are many factors that influence the efficiency of a solar cell. Fig. 4 shows the I-V curves of the COM and REC, whose short-circuit current density ( $J_{sc}$ ), open circuit voltage ( $V_{oc}$ ), fill factor ( $FF$ ), and cell efficiency ( $\eta$ ) are summarized in the inserted table. Even though the COM and REC were fabricated by same cell processing, the results revealed different levels of cell performance. The  $J_{sc}$  and  $V_{oc}$  values of the REC were slightly smaller than those of the COM. Therefore, the cell efficiency of the REC was slightly lower (*i.e.* 0.6%) than that of the COM.

$J_{sc}$  is due to the generation and collection of light-generated carriers. In general, it depends on the optical properties and the collection probability because other factors, such as the number of photons and the spectrum of the incident light, remain more or less constant. For this reason, when comparing solar cells made of the same type of material, the most critical parameters are the optical properties; the transmission and/or reflectance and collection probability; the surface passivation and/or minority carrier lifetime in the base [27]. Among these parameters, surface passivation has little effect on the efficiency of both the COM and REC due to the use of the same conventional cell processing. This means that the low  $J_{sc}$  of REC can be

caused by the transmission and/or reflectance and the minority carrier lifetime in the base.

$V_{oc}$  is the maximum voltage available from a solar cell, which occurs at zero current.  $V_{oc}$  corresponds to the amount of forward bias in the solar cell. It is dependent on the amount of recombination in a p-n junction, and increasing recombination increases the forward bias current [28]. Consequently, high recombination increases the forward bias diffusion current, which in turn reduces  $V_{oc}$ . In order to confirm the cause of the lower  $J_{sc}$  and  $V_{oc}$  value of the REC compared with the COM, the quantum efficiencies were measured.

### 3.4. Quantum efficiency (QE)

QE is the ratio of the number of carriers collected by the solar cell to the number of photons of a given energy incident in the solar cell. The QE for most solar cells is reduced by the recombination effect. The same mechanisms which affect the collection probability also affect the quantum efficiency. To confirm the lower value of  $J_{sc}$  and  $V_{oc}$  in the REC compared with the COM, the external and internal QEs are shown in Fig. 4. The external QE of the REC was smaller than that of the COM at a short wavelength of < 500 nm, as shown in Fig. 5(a). Generally, the external QE of a Si solar cell includes the effect of optical losses such as transmission and reflection. This can be attributed to the high surface reflectance of the solar cell. Fig. 6 shows the measured reflectance and the SEM images of the textured surface of the COM and REC. As can be seen in Fig. 6, the REC has a higher reflectance than the COM of approximately 5% at a short wavelength. It is well known that the deep and large textured pyramidal structures have a low average specular reflectivity [29]. For this reason, the reflectance of the COM is lower compared with the REC, as shown in Fig. 6. This differences between the textured pyramidal structures can be explained by the post-treatment of the Si wafer. In other words, the surface of the REC Si wafer has different characteristics compared with the COM because of acid leaching in the mixed solution. This phenomenon leads to different surface texturing in conventional cell processing. For this reason, the reduction of the REC's external QE at a short wavelength is caused by high reflectance near the surface. As mentioned previously, optical loss is a very important parameter because it influences the  $J_{sc}$  in the solar cell's characteristics. Therefore, it is good agreement that the  $J_{sc}$  of the REC is lower than that of the COM.

The purpose of internal QE is to distinguish between electrical and optical losses, since internal QE represents the QE of the solar cell concerning only those photons which actually generated excess charge carriers [30]. Both the COM and REC were shown to have identical behavior on a long wavelength, as shown in Fig. 5(b). At a short wavelength, however, the IQE result of the REC decreased slightly compared with the COM, which is attributable to an increase of surface recombination and to inclined carrier collection in the emitter region

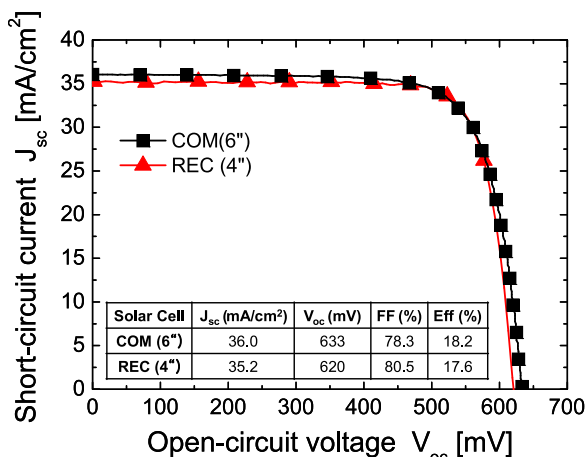


Fig. 4. Light I-V curves of the COM and REC.

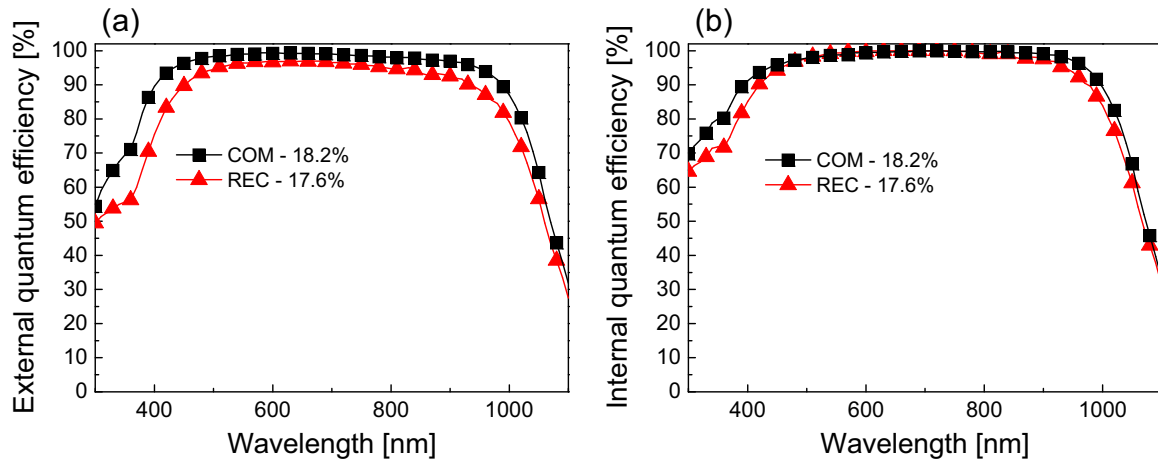


Fig. 5. External and internal quantum efficiencies of the COM and REC.

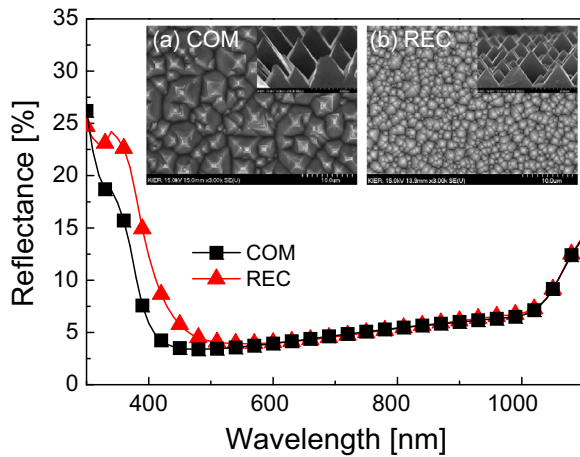


Fig. 6. Reflectance of the COM and REC: The inserted pictures show SEM images of the textured surface: (a) COM (left) and (b) REC (right).

Table 3

The resistivity and minority lifetime of the COM and REC wafers.

	COM	REC
Resistivity (ohm.cm)	2.9	0.72
Minority lifetime ( $\mu$ s)	50.4	7.95

[31]. The  $V_{oc}$  of a Si solar cell is well known to be directly related to the minority lifetime of the Si wafer. For this reason, the  $V_{oc}$  value of the REC was lower than that of the COM. To understand this phenomenon, the resistivity and minority carrier lifetime were evaluated with the COM and REC wafers, as shown in Table 3. The REC wafer was observed to have lower resistivity and minority carrier lifetime compared with the COM wafer, which is usually caused by a high dopant concentration in the bulk Si wafer [32].

### 3.5. Dopants in the solar cell

We analyzed the dopants in the Si wafer – such as P, and B – by GDMS. P dopant was not detected both the COM and the REC. However, the B dopant concentration of the REC was higher than that of the COM in the Si wafer, as shown in Table 4. The high B concentration in the p-type Si is known to lead to a low carrier lifetime. As an explanation for the decrease of the minority carrier lifetime, the dopant plays a key role in the recombination activity within an operating solar cell [33]. The effective lifetime calculated via the

Table 4

Concentration of dopants in the COM and REC wafers measured by GDMS.

Dopant	Concentration (atoms/cc)	
	COM	REC
B	5.0E15	1.0E16
P	< 4.5E15	< 4.5E15

Shockley-Read-Hall mechanism showed a considerable decrease as the dopant density in the Si wafer increased [34]. The calculated effective lifetime decreased considerably from 1000  $\mu$ s at  $1 \times 10^{16} \text{ cm}^{-3}$  doping to 600  $\mu$ s at  $3 \times 10^{16} \text{ cm}^{-3}$  doping, with a donor concentration of  $1 \times 10^{15} \text{ cm}^{-3}$  [35]. This means that such a variation in the minority carrier lifetime could be caused by sensitivity to the presence of defect levels in the band-gap. In other words, this phenomenon is caused by an increase of the recombination center due to the high B dopant concentration [36]. As a result, the higher B concentration results in lower  $V_{oc}$ ,  $J_{sc}$  values and efficiency in the solar cell.

In conclusion, the higher B concentration and reflectance caused by the small textured pyramidal structures of the REC reduces cell efficiency by 0.6 % compared with the COM. However, the REC has sufficient potential for use in the PV industry.

## 4. Conclusion

Various mixing ratios of  $\text{HNO}_3$ :HF were applied in the process of etching the Si solar cells for the recovery of a Si wafer, i.e. 92:8, 75:25, 67:33 and 50:50 at volume fraction. The  $\text{SiN}_x$  and Al back contact on both sides of the solar cell were not completely etched at a low concentration of aqueous HF acid, and the existence of Ag particles on the surface of Si wafer was detected using EDS analysis at a low concentration of aqueous  $\text{HNO}_3$  acid in a mixed solution. A Si wafer that Ag was not detected by EDS analysis could be efficiently obtained under the condition of a mixed acid solution of  $\text{HNO}_3$  and HF at a ratio of 83:17. The recovery of the Si wafer from a 4" EoL solar cell under the optimum etching condition was conducted, and then a 4" c-Si solar cell was fabricated conventionally using the reclaimed Si wafer. The PV performance of the 4" solar cell was evaluated to have a high efficiency of 17.6 %, i.e. a rise of 18.9 % compared with the original efficiency of the solar cell. The REC shows lower  $V_{oc}$  and  $J_{sc}$  values and lower cell efficiency than the COM because of the high reflectance and the high concentration of B dopant.

## Acknowledgement

This work was supported by the Korea Institute of Energy Technology Evaluation and Planning (KETEP) and by the Ministry of Trade, Industry & Energy (MOTIE) of the Republic of Korea (No. 20163010012240). Further support came from the Research and Development Program of the Korea Institute of Energy Research (KIER) (B5-2464).

## References

- [1] S. Kang, S. Yoo, J. Lee, B. Boo, H. Ryu, Experimental investigations for recycling of silicon and glass from waste photovoltaic modules, *Renew. Energy* 47 (2012) 152–159.
- [2] IEA. PVPS, 2014 A Snapshot of Global PV Markets 2014. Rep. IEA PVPS T1-26, 2015
- [3] M.G. Tsoutsouva, V.A. Oliveira, J. Baruchel, D. Camel, B. Marie, T.A. Lafford, Characterization of defects in mono-like silicon for photovoltaic applications using X-ray Bragg diffraction imaging, *J. Appl. Cryst.* 48 (2015) 645–654.
- [4] IEA. PVPS, Review of Failures of Photovoltaic Modules. Rep. IEA-PVPS T13-01, 2014
- [5] V.M. Fthenakis, End-of-life management and recycling of PV modules, *Energy Policy* 28 (2000) 1051–1058.
- [6] A. Ndiaye, A. Charki, A. Kobi, C.M.F. Kebe, P.A. Ndiaye, V. Sambou, Degradations of silicon photovoltaic modules: a literature review, *Sol. Energy* 96 (2013) 140–151.
- [7] N.C. McDonald, J.M. Pearce, Producer responsibility and recycling solar photovoltaic modules, *Energy Policy* 38 (2010) 7041–7047.
- [8] Y.K. Yi, H.S. Kim, T. Tran, S.K. Hong, M.J. Kim, Recovering valuable metals from recycled photovoltaic modules, *J. Air Waste Manag.* 64 (7) (2014) 797–807.
- [9] S. Dubey, N.Y. Jadhav, B. Zakirova, Socio-economic and environmental impacts of silicon based photovoltaic (PV) technologies, *Energy Procedia* 33 (2013) 322–334.
- [10] C. Olson, B. Geerligs, M. Goris, I. Bennett, J. Clyncke, Current and future priorities for mass and material in silicon pv module recycling, in: *Proceedings of 28th EU PVSEC*, 30, 2013 pp. 4629–4633.
- [11] C.H. Lee, C.E. Hung, S.L. Tsai, S.R. Popuri, C.H. Liao, Resource recovery of scrap silicon solar battery cell, *Waste Manag. Res.* 31 (5) (2013) 518–524.
- [12] J. Zhang, F. Lv, L.Y. Ma, L.J. Yang, The Status and Trends of Crystalline Silicon PV Module Recycling Treatment Methods in Europe and China, *Adv. Mat. Res.* 724–725 (2013) 200–204.
- [13] Directive E.C., Directive 2012/19/EU of the European Parliament and of the Council of 4 July 2012 on waste electrical and electronic equipment (WEEE), *Official Journal of the European Union L* 197 (2012) 38–71.
- [14] G. Granata, F. Pagnanelli, E. Moscardini, T. Havlik, L. Toro, Recycling of photovoltaic panels by physical operations, *Sol. Energy Mater. Sol. C* 123 (2014) 239–248.
- [15] J.S. Lee, Y.S. Ahn, B.Y. Jang, J.S. Kim, G.H. Kang, Disassembling photovoltaic module, US Granted Patent No. 9455367 B2
- [16] E. Klugmann-Radziemska, P. Ostrowski, K. Drabczyk, P. Panek, M. Szkodo, Experimental validation of crystalline silicon solar cells recycling by thermal and chemical methods, *Sol. Energy Mater. Sol. C* 94 (2010) 2275–2282.
- [17] E. Klugmann-Radziemska, P. Ostrowski, Chemical treatment of crystalline silicon solar cells as a method of recovering pure silicon from photovoltaic modules, *Renew. Energy* 35 (2010) 1751–1759.
- [18] J. Park, N. Park, Wet etching processes for recycling crystalline silicon solar cells from end-of-life photovoltaic modules, *RSC Adv.* 4 (2014) 34823–34829.
- [19] E. Radziemska, P. Ostrowski, A. Cenian, M. Sawczak, Chemical, thermal and laser processes in recycling of photovoltaic silicon solar cells and modules, *Ecol. Chem. Eng. S* 17 (3) (2010) 385–391.
- [20] H. Ritala, J. Kiihamäki, M. Heikkilä, Studies on aluminium corrosion during and after HF vapour treatment, *Microelectron. Eng.* 87 (2010) 501–504.
- [21] S.K. Sadrnezhad, E. Ahmadi, M. Mozammel, Kinetics of silver dissolution in nitric acid from Ag-Au<sub>0.04</sub>-Cu<sub>0.10</sub> and Ag-Cu<sub>0.23</sub> scraps, *J. Mater. Sci. Technol.* 22 (5) (2006) 696–700.
- [22] M. Steinert, J. Acker, S. Oswald, K. Wetzig, Study on the mechanism of silicon etching in HNO<sub>3</sub>-Rich HF/HNO<sub>3</sub> mixtures, *J. Phys. Chem. C* 111 (2007) 2133–2140.
- [23] M. Abouda-Lachiheb, N. Nafie, M. Bouaicha, The dual role of silver during silicon etching in HF solution, *Nanoscale. Res. Lett.* 7 (1) (2012) 1–5.
- [24] H. Tong, C.M. Wang, W.C. Ye, Y.L. Chang, H.L. Li, Study of the electroless silver seed formation on silicon surface, *Chin. J. Chem.* 25 (2007) 208–212.
- [25] H. Morinaga, M. Suyama, T. Ohmi, Mechanism of metallic particle growth and metal-induced pitting on Si wafer surface in wet chemical processing, *J. Electrochem. Soc.* 141 (10) (1994) 2834–2841.
- [26] C.J.J. Tool, A.R. Burgers, P. Manshanden, A.W. Weeber, B.H.M. van Straaten, Influence of wafer thickness on the performance of multicrystalline Si solar cells: an experimental study, *Prog. Photovolt.: Res. Appl.* 10 (2002) 279–291.
- [27] A. Ibrahim, M.R.I. Ramadan, S. Aboul-Enein, A. ElSebaei, S.M. El-Broulesy, Short circuit current  $i_{sc}$  as a real non-destructive diagnostic tool of a photovoltaic modules performance, *Int. J. Renew. Energy Res. (IJRER)* 1 (2011) 53–59.
- [28] C.T. Dervos, P.D. Skafidas, J.A. Mergos, P. Vassiliou, p-n junction photocurrent modelling evaluation under optical and electrical excitation, *Sensors* 5 (2004) 58–70.
- [29] S.M. Iftiqar, Y. Lee, M. Ju, N. Balaji, S.K. Dhungel, J. Yi, Fabrication of Crystalline Silicon Solar Cell with Emitter Diffusion, SiN<sub>x</sub> Surface Passivation and Screen Printing of Electrode. *Intech Open Access Publisher*, 2012, pp. 105–132
- [30] M. Padilla, B. Michl, B. Thaidigsmann, W. Warta, M.C. Schubert, Short-circuit current density mapping for solar cells, *Sol. Energy Mater. Sol. C* 120 (2014) 282–288.
- [31] L. Peng, H. Pei-De, F. Yu-Jie, X. Yu-Peng, Boron implanted emitter for n-type silicon solar cell, *Chin. Phys. B* 24 (3) (2015) 038801.
- [32] K. Bothe, R. Sinton, J. Schmidt, Fundamental boron–oxygen-related carrier lifetime limit in mono- and multicrystalline silicon, *Prog. Photovolt.: Res. Appl.* 13 (2005) 287–296.
- [33] D.L. Meier, J. Hwang, R.B. Campbell, The effect of doping density and injection level on minority-carrier lifetime as applied to bifacial dendritic web silicon solar cells, *IEEE. Trans. Electron Devices* 35 (1) (1988) 70–79.
- [34] A. Cuevas, D. Macdonald, Measuring and interpreting the lifetime of silicon wafers, *Sol. Energy* 76 (2004) 255–262.
- [35] D. Macdonald, A. Cuevas, Recombination in compensated crystalline silicon for solar cells, *J. Appl. Phys.* 109 (2011) 043704.
- [36] E. Gaubas, J. Vanhellemont, Comparative study of carrier lifetime dependence on dopant concentration in silicon and germanium, *J. Electrochem. Soc.* 154 (2007) H231–H238.